

Graph Chirp Signal and Graph Fractional Vertex-Frequency Energy Distribution

Manjun Cui and Zhichao Zhang, *Member, IEEE*

Abstract—Graph signal processing (GSP) has emerged as a powerful framework for analyzing data on irregular domains. In recent years, many classical techniques in signal processing (SP) have been successfully extended to GSP. Among them, chirp signals play a crucial role in various SP applications. However, graph chirp signals have not been formally defined despite their importance. Here, we define graph chirp signals and establish a comprehensive theoretical framework for their analysis. We propose the graph fractional vertex-frequency energy distribution (GFED), which provides a powerful tool for processing and analyzing graph chirp signals. We introduce the general fractional graph distribution (GFGD), a generalized vertex-frequency distribution, and the reduced interference GFED, which can suppress cross-term interference and enhance signal clarity. Furthermore, we propose a novel method for detecting graph signals through GFED domain filtering, facilitating robust detection and analysis of graph chirp signals in noisy environments. Moreover, this method can be applied to real-world data for denoising more effectively than some state-of-the-arts, further demonstrating its practical significance.

Index Terms—Chirp signal, filtering, general fractional graph distribution, graph fractional vertex-frequency energy distribution, signal detection.

I. INTRODUCTION

Graph signal processing (GSP) is an emerging field that analyzes and processes signals defined on irregular graph structures [1]–[3]. It extends traditional signal processing (SP), which typically operates in Euclidean domains, to non-Euclidean domains, facilitating the analysis of data from networks such as social, sensor, and biological systems, where traditional SP may be inadequate [1], [4]–[7].

In SP, the fractional Fourier transform (FRFT) [8], [9] is a generalization of the classical Fourier transform (FT) [10], [11] that facilitates a more flexible analysis of signals in different

fractional domains. The FRFT is an effective tool for analyzing and processing linear frequency modulation (LFM) signals, also known as chirp signals, which are characterized by their frequency variation over time [8], [12]–[15]. In GSP, the graph Fourier transform (GFT) [2], [4], [5], [16] can be extended to graph fractional Fourier transform (GFRFT) [17], [18] by introducing the fractional parameter a , thereby facilitating a more sophisticated signal analysis in fractional domains defined on graphs. While the FRFT has been extensively studied for chirp signals, the concept of graph chirp signal remains absent in the realm of GSP. Defining such a signal is crucial for enhancing the analytical capabilities of GSP.

Time-frequency analysis is a fundamental technique in SP [19], [20]. Time-frequency distributions provide simultaneous representations of signals' attributes in the combined time-frequency domain, enabling a more comprehensive analysis of signals with time-varying frequency content. Among these distributions, the Wigner-Ville distribution (WD) stands out as one of the most widely used [21]–[23], due to its high resolution, making it particularly effective for capturing the instantaneous frequency and temporal dynamics of signals. In the realm of GSP, however, there is no direct extension of the WD for analyzing signals defined on graphs. Despite this, the graph vertex-frequency energy distribution (GED) can fulfill a similar role. In GSP, the GED [24], [25], known as the vertex-frequency distribution, characterizes the energy distribution within a graph signal across its vertices and frequency components. This distribution is analogous to the Rihaczek distribution [26], [27] in time-frequency analysis.

In classical SP, the relationship between WD and FRFT reflects a rotation in the time-frequency plane [8], making it particularly useful for analyzing chirp signals. Fractionalizing the WD enriches the structure of the time-frequency plane, thereby enhancing the performance of signal analysis, such as in signal detection and filtering [28]–[32]. Conversely, no analogous rotational relationship exists between the GED and the GFRFT. Thus, these methods are not typically suitable for analyzing graph chirp signals. However, fractionalizing the GED enhances the structure of the vertex-frequency plane, making it more complex and enriched, and thus better suited for analyzing graph chirp signals.

In SP, the Cohen's class time-frequency distribution (CD) is one of the most comprehensive bi-linear kernel time-frequency distributions in SP [20]. When the kernel function is set to 1, the CD degenerates into the well-known WD, which, despite its widespread applications, still contains cross-terms that can introduce interference in time-frequency plane. Thus, researchers have focused on designing different kernel

This work was supported in part by the Foundation of Key Laboratory of System Control and Information Processing, Ministry of Education under Grant Scip20240121; in part by the Foundation of Key Laboratory of Computational Science and Application of Hainan Province under Grant JSKX202401; and in part by the Postgraduate Research & Practice Innovation Program of Jiangsu Province under Grant KYCX24_1405. (*Corresponding author: Zhichao Zhang.*)

Manjun Cui is with the School of Mathematics and Statistics, the Center for Applied Mathematics of Jiangsu Province, and the Jiangsu International Joint Laboratory on System Modeling and Data Analysis, Nanjing University of Information Science and Technology, Nanjing 210044, China (e-mail: cmj1109@163.com).

Zhichao Zhang is with the School of Mathematics and Statistics, Nanjing University of Information Science and Technology, Nanjing 210044, China, with the Key Laboratory of System Control and Information Processing, Ministry of Education, Shanghai Jiao Tong University, Shanghai 200240, China, and also with the Key Laboratory of Computational Science and Application of Hainan Province, Hainan Normal University, Haikou 571158, China (e-mail: zzc910731@163.com).

functions to suppress these cross-terms [33]–[38]. The CD in GSP aligns with the general graph distribution (GGD). Likewise, the GGD can be fractionalized, facilitating a more nuanced representation in the vertex-frequency domain. This fractionalization helps to better manage and suppress cross-terms interference, improving the accuracy of graph signal analysis.

In summary, the analysis of graph chirp signals is crucial in GSP. The main objective of this paper is to define graph chirp signals and provide a tool for processing them by extending the GED and integrating it with the GFRFT to develop a fractionalized GED, thereby enhancing the theoretical framework for graph signal analysis. This approach offers an effective framework for analyzing and processing graph chirp signals with the potential to significantly impact the field of SP and graph theory, underscoring its significance to the audience. The main contributions of this paper are summarized as follows:

- This paper defines the graph chirp signal.
- This paper defines the graph fractional vertex-frequency energy distribution (GFED) and presents its corresponding properties.
- This paper defines the general fractional graph distribution (GFGD) and presents its corresponding properties. Moreover, this paper gives some examples of reduced interference GFED.
- This paper proposes a method for chirp signal detection using filtering in the GFED domain. Furthermore, the method can be applied to real-world scenarios for denoising more effective than some state-of-the-arts.

The remainder of this paper is organized as follows. Section II introduces some preliminary concepts. Section III defines graph chirp signals and discusses their relevant properties. Section IV presents the definition and properties of the GFED. Section V introduces the GFGD and the reduced interference GFED. Section VI proposes a method for detecting graph chirp signals using filtering in the GFED domain. Section VII provides numerical experiments on the detection of graph chirp signals and the filtering of real-world data. Finally, Section VIII concludes the paper. Fig. 1 presents a mind map delineating the framework and principal concepts of this paper. All the technical proofs of our theoretical results are relegated to the Appendix parts.

II. PRELIMINARIES

A. Graph Fourier transform

Let $\mathcal{G} = \{\mathcal{N}, \mathcal{E}, \mathbf{A}\}$ be a graph or network with a set of N nodes \mathcal{N} , edges \mathcal{E} such that $(m, n) \in \mathcal{E}$ and the graph adjacency \mathbf{A} . If there is no edge from node n to node m , the element $\mathbf{A}_{mn} = 0$, otherwise $\mathbf{A}_{mn} = 1$. The matrix \mathbf{W} represents the strength of the connections between the nodes in the graph, where each element W_{mn} denotes the weight of the edge between nodes m and n . The diagonal elements W_{nn} are zeros. The Laplacian is defined as $\mathbf{L} = \mathbf{D} - \mathbf{W}$, where \mathbf{D} is the diagonal degree matrix with $D_{nn} = \sum_{m=1}^N W_{nm}$. For any undirected graph, the Laplacian is symmetric, i.e. $\mathbf{L} = \mathbf{L}^T$. A graph signal $\mathbf{x} = [x(1), x(2), \dots, x(N)]^T$, $\mathbf{x} \in \mathbb{C}^N$, is

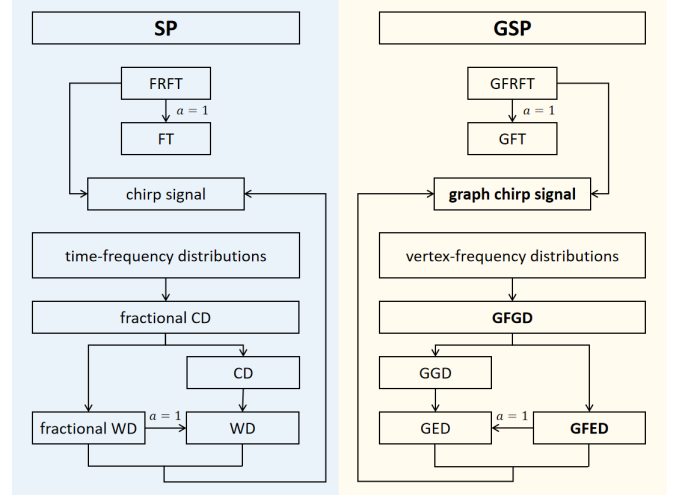


Fig. 1. The framework and principal concepts of the paper, focusing on the relationship between SP and GSP.

defined as a mapping from the set of vertices \mathcal{N} to \mathbb{C}^N , i.e. $\mathcal{N}_n \rightarrow x(n)$.

In [2], the GFT is defined using the general graph shift operator (GSO) \mathbf{Z} (e.g. adjacency \mathbf{A} , weighted adjacency \mathbf{W} , Laplacian \mathbf{L} , row normalized adjacency, symmetric normalized Laplacian). The GSO \mathbf{Z} can be decomposed as $\mathbf{Z} = \mathbf{U}\mathbf{\Lambda}\mathbf{U}^{-1}$, where \mathbf{U} is the matrix whose columns are the eigenvectors \mathbf{u}_k , $k = 1, 2, \dots, N$, and $\mathbf{\Lambda}$ is the diagonal matrix consisting of eigenvalues $\lambda_1, \lambda_2, \dots, \lambda_N$ on the diagonal. It is obvious that \mathbf{U} is unitary, unless explicitly stated, the decomposition is based on the graph Laplacian in this paper.

The GFT of a signal \mathbf{x} is defined as

$$\hat{\mathbf{x}} = \mathbf{F}_G \mathbf{x} = \mathbf{U}^{-1} \mathbf{x}, \quad (1)$$

where $\mathbf{F}_G = \mathbf{U}^{-1}$ is the GFT matrix and $\hat{\mathbf{x}} = [\hat{x}(1), \hat{x}(2), \dots, \hat{x}(N)]$ denotes the GFT vector with $\hat{x}(k) = \sum_{n=1}^N x(n) u_k(n)$. Here, the superscript \ast denotes the complex conjugate operator.

The inverse GFT is defined as

$$\mathbf{x} = \mathbf{F}_G^{-1} \hat{\mathbf{x}} = \mathbf{U} \hat{\mathbf{x}}, \quad (2)$$

with $x(n) = \sum_{k=1}^N \hat{x}(k) u_k(n)$.

B. Graph fractional Fourier transform

By performing the Jordan decomposition on the GFT matrix \mathbf{F}_G , we express it as $\mathbf{F}_G = \mathbf{P}\mathbf{J}_F\mathbf{P}^{-1}$, where \mathbf{P} is the matrix of generalized eigenvectors and \mathbf{J}_F is the Jordan canonical form of \mathbf{F}_G . This decomposition allows us to obtain the GFRFT matrix \mathbf{F}_G^a of order a as follows:

$$\mathbf{F}_G^a = \mathbf{P}\mathbf{J}_F^a\mathbf{P}^{-1} \quad (3)$$

The a th order GFRFT of any signal \mathbf{x} is defined as [17]

$$\hat{\mathbf{x}}_a = \mathbf{F}_G^a \mathbf{x}, \quad (4)$$

where $\hat{\mathbf{x}}_a = (\hat{x}_a(1), \hat{x}_a(2), \dots, \hat{x}_a(N))$ is the GFRFT vector. It is obvious that the GFRFT matrices satisfy index additivity,

that is $\mathbf{F}_G^a \mathbf{F}_G^b = \mathbf{F}_G^{a+b}$. Thus, the inverse GFRFT can be defined as

$$\mathbf{x} = (\mathbf{F}_G^a)^{-1} \widehat{\mathbf{x}}_a. \quad (5)$$

The GFRFT matrix \mathbf{F}_G^a reduces to the unit matrix \mathbf{I}_N for $a = 0$, and the GFT matrix \mathbf{F}_G for $a = 1$.

III. THE GRAPH CHIRP SIGNAL

LFM signal, also known as chirp signal, characterized by a frequency that varies with time, have long been utilized in classical SP for applications such as radar, communications, and system identification. A chirp signal typically exhibits a frequency that changes linearly with time.

In the continuous domain, a LFM signal is defined as [12], [13]

$$f(t) = e^{i(f_0 t + \frac{f_k}{2} t^2)} \quad (6)$$

where f_0 and f_k denote the initial frequency and chirp rate, respectively.

As is known to all, the fractional Fourier transform [39], [40] of a chirp signal generates a characteristic spike, often referred to as an impulse. Thus, we can extend the idea of chirp signals to the graph domain and define the graph chirp signal.

Definition 1: For a graph or network \mathcal{G} with the GFT matrix \mathbf{F}_G , the graph chirp signal \mathbf{u}_k^a is defined as the k th column of the inverse of a order GFRFT matrix, as follows:

$$\mathbf{u}_k^a = (\mathbf{F}_G^a)^{-1}(:, k), \quad (7)$$

where a is the graph chirp rate and k is the graph initial frequency.

To provide a clearer illustration of the behavior of chirp signals, in Fig. 2, we give examples on four different graph structures: the David sensor, Swiss roll, comet, and low-stretch tree. For each graph, we examine the behavior of chirp signals with varying parameters, specifically the chirp rates $a = \{0.3, 0.5, 0.8\}$, as well as initial frequencies $k = \{1, 30, 50\}$. Each graph contains $N = 64$ vertices.

The adjacency matrix of a cycle graph is given by

$$\mathbf{A} = \begin{bmatrix} 1 & & & & 1 \\ & \ddots & & & \\ & & \ddots & & \\ & & & \ddots & \\ & & & & 1 \end{bmatrix}. \quad (8)$$

On a cycle graph, the GFRFT matrix, \mathbf{F}_G^a , is equal to the discrete fractional Fourier transform (DFRDT) matrix [17]. Consequently, the graph chirp signals on a cycle graph are defined as the columns of the DFRFT matrix with a fractional order $-a$. Fig. 3 illustrates the graph chirp signals on a cycle graph with $N = 20$ vertices for chirp rates $a = \{0.3, 0.5, 0.8\}$ and initial frequencies $k = \{1, 9, 18\}$.

The GFRFT of a graph chirp signal \mathbf{u}_k^a produces a corresponding impulse in the graph fractional spectral domain, analogous to the chirp signal's behavior in classical SP. For simplicity, let $\mathbf{U}_a = (\mathbf{u}_1^a, \mathbf{u}_2^a, \dots, \mathbf{u}_N^a)$.

For example, Fig. 4 illustrates the GFRFT of the chirp signal $\mathbf{u}_{50}^{0.5}$ on the David sensor, with the fractional order a varying from 0.1 to 1. As can be seen, the GFRFT for this

fractional order generates an impulse at the chirp rate $a = 0.5$, indicating that the signal exhibits a well-defined frequency concentration at this order. At other fractional orders, the spectrum is more mixed. The GFRFT effectively handles graph chirp signals by providing a flexible method to adjust the order. This aligns with the classical treatment of chirp signals, where the frequency evolution over time is captured precisely.

IV. FRACTIONAL VERTEX-FREQUENCY ENERGY DISTRIBUTION

A. Vertex-frequency energy distribution

In classical SP, the WD [21], [22] is a well-known tool that provides a joint representation of a signal, offering valuable insight into its time-frequency characteristics. It is particularly effective for the analysis and processing of LFM signals, such as filtering and detection. In GSP, the concept of energy distribution holds an analogous importance to the role of WD in classical SP.

In [24], the GED is proposed, which corresponds to the Rihaczek distribution in time-frequency analysis and is defined as follows:

$$E_{\mathbf{x}}(n, k) = x(n) \overline{\widehat{x}(k)} \overline{u_k(n)}. \quad (9)$$

It satisfies the marginal properties:

$$\sum_{n=1}^N E_{\mathbf{x}}(n, k) = |\widehat{x}(k)|^2, \quad (10)$$

$$\sum_{k=1}^N E_{\mathbf{x}}(n, k) = |x(n)|^2. \quad (11)$$

B. Fractional vertex-frequency energy distribution

The energy of a signal in classical SP \mathbf{x} is

$$E_{\mathbf{x}} = \sum_{n=1}^N |x(n)|^2. \quad (12)$$

To preserve the energy, the above equation can be rewritten through GFRFT as

$$E_{\mathbf{x}} = \sum_{n=1}^N \sum_{k=1}^N x(n) \overline{\widehat{x}_a(k)} \overline{u_k^a(n)}. \quad (13)$$

Thus, we can define the GFED to further enhance the flexibility of signal analysis on graphs.

Definition 2: For the signal \mathbf{x} defined on the graph \mathcal{G} , the GFED $E_{\mathbf{x}}^a$ of order a is defined as

$$\begin{aligned} E_{\mathbf{x}}^a(n, k) &= x(n) \overline{\widehat{x}_a(k)} \overline{u_k^a(n)} \\ &= \sum_{m=1}^N x(n) \overline{\widehat{x}_a(m)} \overline{u_k^a(m)} \end{aligned} \quad (14)$$

When $a = 1$, the GFED reduces to the GED. Obviously, the GFED satisfies the marginal properties as well.

Vertex marginal property:

$$\sum_{k=1}^N E_{\mathbf{x}}^a(n, k) = |x(n)|^2. \quad (15)$$

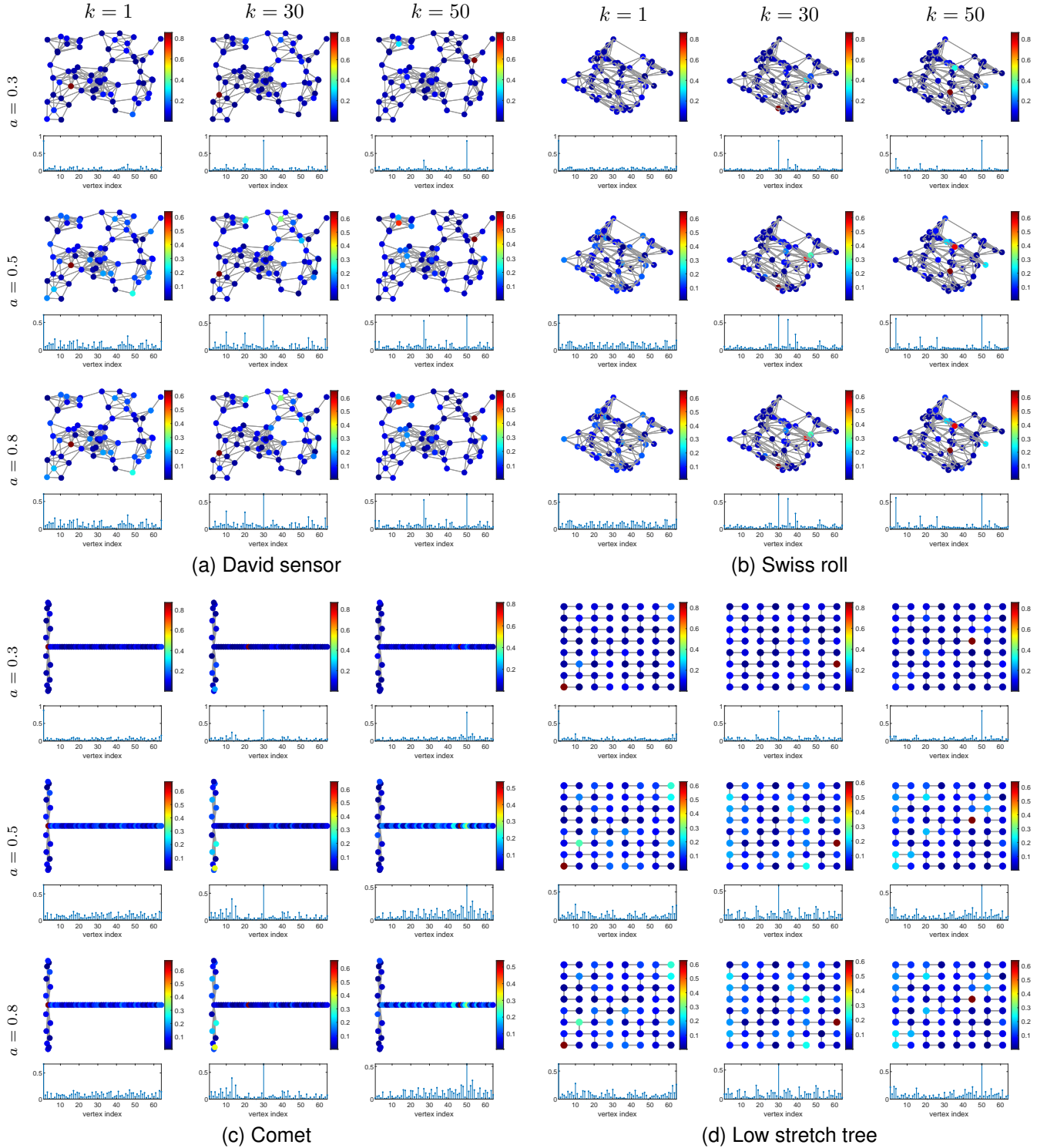


Fig. 2. Graph chirp signals with different chirp rates and initial frequencies on four graph structures. (a) David sensor. (b) Swiss roll. (c) Comet. (d) Low stretch tree.

Frequency marginal property:

$$\sum_{n=1}^N E_{\mathbf{x}}^a(n, k) = |\hat{x}_a(k)|^2. \quad (16)$$

Example 1: Consider a sensor network graph presented in Fig. 1(a). The graph chirp frequency $a = 0.7$ is selected for the

graph chirp signals, with initial frequencies chosen as follows. The graph signal \mathbf{x}_1 , is defined on vertices 1 to 34 using the graph chirp signal \mathbf{u}_{10}^a , and on vertices 35 to 64 using \mathbf{u}_{54}^a , along with an additional \mathbf{u}_{33}^a . The graph signal \mathbf{x}_2 , is defined on vertices 1 to 24 using \mathbf{u}_{22}^a , on vertices 25 to 34 using \mathbf{u}_7^a , and on vertices 35 to 64 using \mathbf{u}_{42}^a , along with the additional \mathbf{u}_{33}^a . The GEDs and GFEDs, along with the

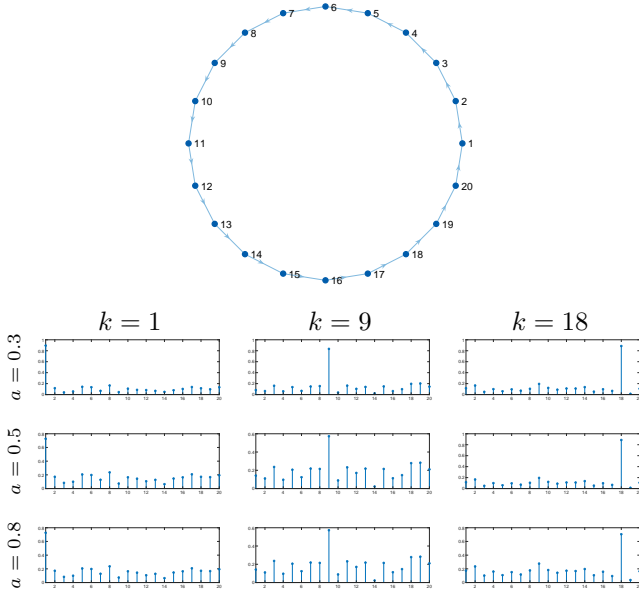


Fig. 3. Graph chirp signals with different chirp rates and initial frequencies on cycle graph.

marginal properties are illustrated in Fig. 5.

Example 2: Consider a community network graph presented in Fig. 2(a). The graph chirp frequency $a = 0.6$ is selected for the graph chirp signals, with initial frequencies chosen as follows. The graph signal \mathbf{x}_3 , is defined on vertices 1 to 27 using the graph chirp signal \mathbf{u}_{37}^a , and on vertices 28 to 64 using \mathbf{u}_{37}^a , along with an additional \mathbf{u}_{29}^a . The graph signal \mathbf{x}_4 , is defined on vertices 1 to 10 using \mathbf{u}_6^a , on vertices 11 to 27 using \mathbf{u}_{15}^a , and on vertices 28 to 64 using \mathbf{u}_{51}^a , along with the additional \mathbf{u}_{29}^a . The GEDs and GFEDs, along with the marginal properties are illustrated in Fig. 6.

As demonstrated in Examples 1 and 2, the GEDs fail to adequately capture the characteristics of graph chirp signals. In contrast, the GFEDs provide superior performance, effectively revealing vertex-frequency information, accurately identifying initial frequency components, and achieving greater energy concentration.

V. GENERAL FRACTIONAL GRAPH DISTRIBUTION

The GGD form is [41]

$$G_{\mathbf{x}}(n, k) = \sum_{p=1}^N \sum_{q=1}^N \widehat{x}(p) \overline{\widehat{x}(q)} u_p(n) \overline{u_q(n)} \phi(p, k, q), \quad (17)$$

where ϕ is the kernel function.

When $\phi(p, k, q) = \delta(q - k)$, the GGD reduces to the GED. Additionally, if the kernel satisfies the condition $\sum_{k=1}^N \phi(p, k, q) = 1$, the unbiased condition holds, i.e. $\sum_{n=1}^N \sum_{k=1}^N G_{\mathbf{x}}(n, k) = E_{\mathbf{x}}$.

To further extend the GGD, next, we introduce the GFGD.

Definition 3: For the signal \mathbf{x} defined on the graph \mathcal{G} , the GFGD $G_{\mathbf{x}}^a$ of order a is defined as

$$G_{\mathbf{x}}^a(n, k) = \sum_{p=1}^N \sum_{q=1}^N \widehat{x}_a(p) \overline{\widehat{x}_a(q)} u_p^a(n) \overline{u_q^a(n)} \phi(p, k, q). \quad (18)$$

It is evident that when $a = 1$, the GFGD reduces to the GGD. Moreover, when $\phi(p, k, q) = \delta(q - k)$, the GFGD reduces to the GFED. Additionally, the unbiased energy condition $\sum_{n=1}^N \sum_{k=1}^N G_{\mathbf{x}}^a(n, k) = E_{\mathbf{x}}$ holds if $\sum_{k=1}^N \phi(p, k, q) = 1$.

The GFGD satisfies the vertex and frequency marginal properties as follows:

Vertex marginal property:

If $\sum_{k=1}^N \phi(p, k, q) = 1$, the GFGD satisfies the vertex marginal property

$$\begin{aligned} \sum_{k=1}^N G_{\mathbf{x}}^a(n, k) &= \sum_{p=1}^N \sum_{q=1}^N \widehat{x}_a(p) \overline{\widehat{x}_a(q)} u_p^a(n) \overline{u_q^a(n)} \\ &= |x(n)|^2. \end{aligned} \quad (19)$$

Also, the vertex moment property $\sum_{n=1}^N \sum_{k=1}^N n^m G_{\mathbf{x}}^a(n, k) = \sum_{n=1}^N n^m |x(n)|^2$ holds for the same condition.

Frequency marginal property:

If $\phi(p, k, p) = \delta(p - k)$, the GFGD satisfies the frequency marginal property

$$\sum_{n=1}^N G_{\mathbf{x}}^a(n, k) = \sum_{p=1}^N |\widehat{x}_a(p)|^2 \phi(p, k, p) = |\widehat{x}_a(k)|^2. \quad (20)$$

Also, the frequency moment property $\sum_{n=1}^N \sum_{k=1}^N n^m G_{\mathbf{x}}^a(n, k) = \sum_{k=1}^N k^m |\widehat{x}_a(k)|^2$ holds for the same condition.

Additionally, the GFGD can be rewritten as a dual form of (18) in the vertex-vertex domain as

$$G_{\mathbf{x}}^a(n, k) = \sum_{m=1}^N \sum_{t=1}^N x(m) \overline{x(t)} u_k^a(m) \overline{u_k^a(t)} \varphi(m, n, t), \quad (21)$$

where $\varphi(m, n, t)$ is the kernel function in this domain, which has the same mathematical form with the frequency-frequency domain kernel in essence. Furthermore, if $\varphi(m, n, t) = \delta(m - n)$, the vertex marginal property is satisfied. Similarly, if $\sum_{n=1}^N \varphi(m, n, t) = 1$, the frequency marginal property is satisfied.

The form of Choi-Williams kernel in GSP is [41]

$$\phi(p, k, q) = \frac{1}{s(p, q)} e^{-\gamma \frac{|\lambda_k - \lambda_q|}{|\lambda_p - \lambda_q|}} \quad (22)$$

where $s(p, q) = \sum_{k=1}^N e^{-\gamma \frac{|\lambda_k - \lambda_q|}{|\lambda_p - \lambda_q|}}$ for $p \neq q$ and $s(p, q) = \delta(p - q)$ for $p = q$. The reduced interference GFED using the Choi-Williams kernel satisfies the marginal properties.

For the signals used in Examples 1–4, Fig. 7 plots the GGD with Choi-Williams kernel (GGD-CW) and GFGD with Choi-Williams kernel (GFGD-CW) of these four signals. Specifically, Figs. 3(a)–3(d) display the GGD-CW of the four signals, while Figs. 3(e)–3(h) display the GFGD-CW of the same signals.

As can be seen from Fig. 7, the GGD-CWs help reduce interference in the GEDs for signals shown in Figs. 5 and 6. However, they fail to correctly display the corresponding frequency components, as many other frequency components interfere the analysis. In contrast, the GFGD-CWs not only

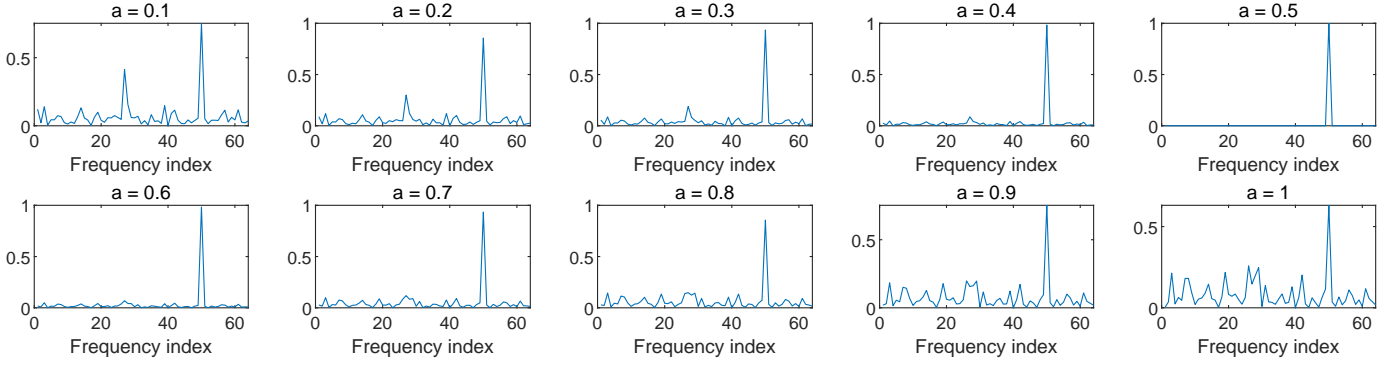
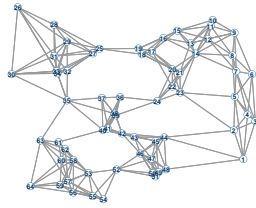
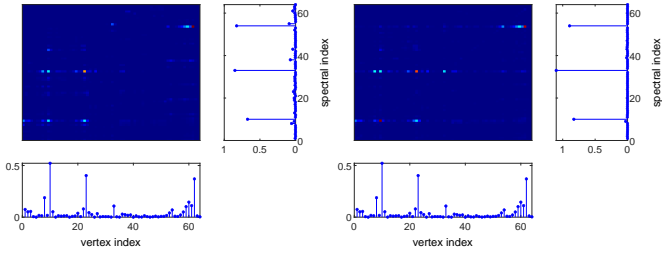


Fig. 4. GFRFTs of the chirp signal on David sensor ($a = 0.5$, $k = 50$) at different fractional orders.

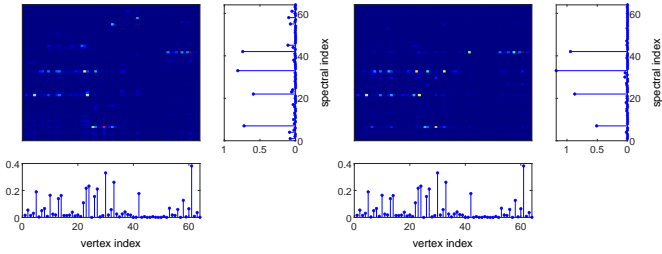


(a)



(b)

(c)



(d)

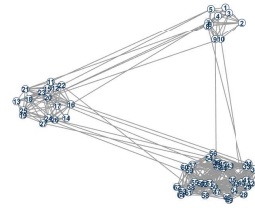
(e)

Fig. 5. Sensor network graph structure and GFEDs. (a) Graph structure. (b) The GED of x_1 . (c) The GFED of x_1 ($a = 0.7$). (d) The GED of x_2 . (e) The GFED of x_2 ($a = 0.7$).

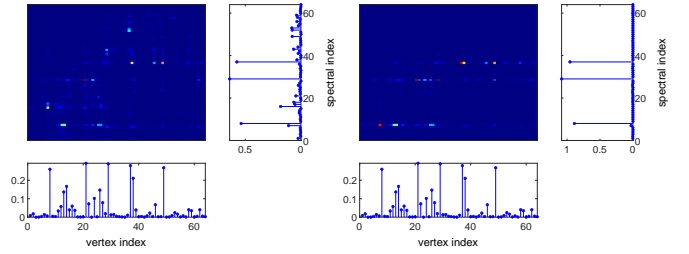
perform better in suppressing cross-terms in the GFEDs, but also provide a clearer representation of the vertex-fractional-frequency components, offering a more accurate depiction of the signals.

VI. DETECTION OF GRAPH SIGNALS THROUGH FRACTIONAL VERTEX-FREQUENCY ENERGY DISTRIBUTION DOMAIN FILTERING

Filtering and detecting play crucial roles in GSP, as they help in extracting relevant information while reducing un-

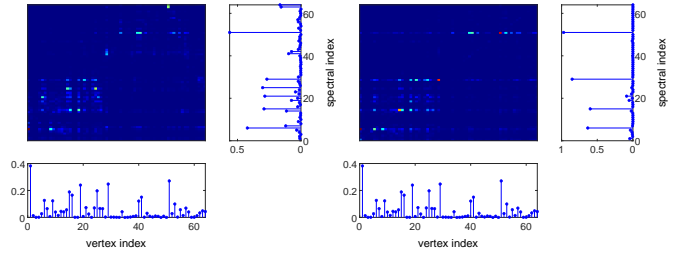


(a)



(b)

(c)



(d)

(e)

Fig. 6. Community network graph structure and GFEDs. (a) Graph structure. (b) The GED of x_3 . (c) The GFED of x_3 ($a = 0.6$). (d) The GED of x_4 . (e) The GFED of x_4 ($a = 0.6$).

wanted noise. Typically, filtering is performed either in the vertex domain or in the frequency domain. In this section, we focus on signal detection through filtering techniques in the vertex-frequency domain, a hybrid approach that combines the strengths of both the vertex and frequency domains.

For the pure and noisy signals x and y , we use the signal observation model $y = x + w$, where w represents the additive noise. According to Wiener filter principle, a natural criterion

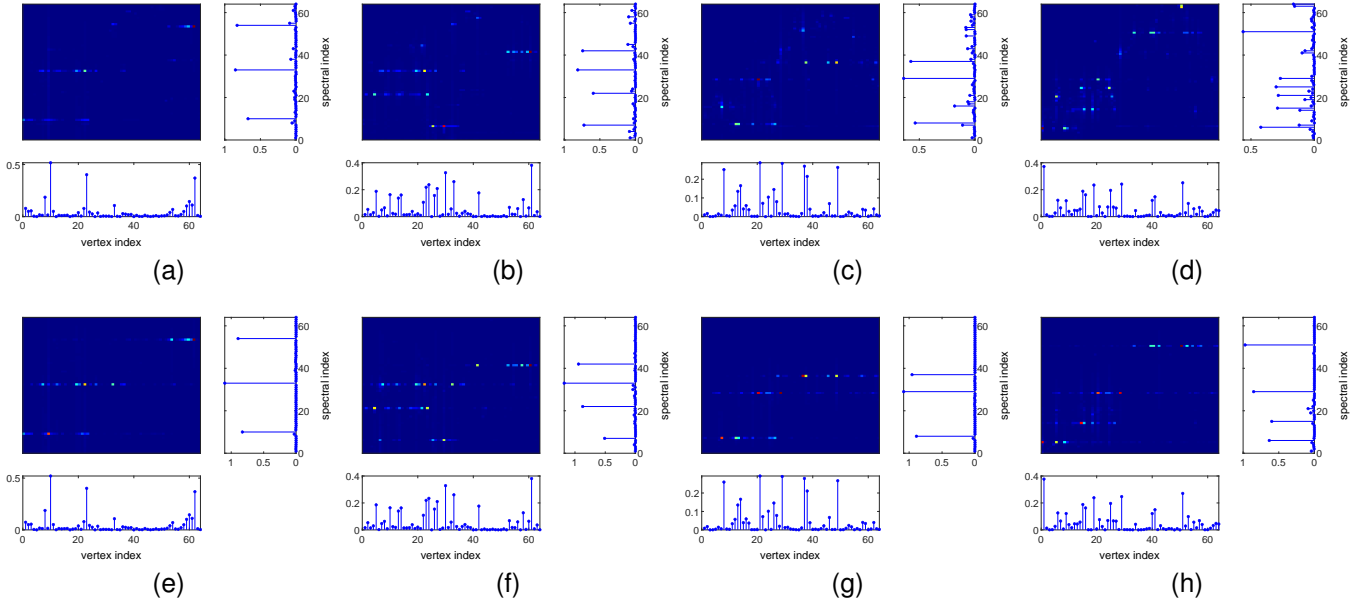


Fig. 7. The GGD-CWs and GFGD-CWs of the four signals. (a) The GGD-CW of \mathbf{x}_1 . (b) The GGD-CW of \mathbf{x}_2 . (c) The GGD-CW of \mathbf{x}_3 . (d) The GGD-CW of \mathbf{x}_4 . (e) The GFGD-CW of \mathbf{x}_1 ($a = 0.7$). (f) The GFGD-CW of \mathbf{x}_2 ($a = 0.7$). (g) The GFGD-CW of \mathbf{x}_3 ($a = 0.6$). (h) The GFGD-CW of \mathbf{x}_4 ($a = 0.6$).

to characterize the estimation accuracy is the MSE criterion

$$\text{MSE} = \mathbb{E} \left\{ \|E_{\mathbf{x}}^a - E_{\hat{\mathbf{x}}}^a\|_F^2 \right\}. \quad (23)$$

where \mathbb{E} denotes the mathematical expectation operator and $E_{\hat{\mathbf{x}}}^a$ is the estimated GFED. We can then formulate the problem as

$$\sigma_{\text{MSE}}^2 = \min_{\mathbf{H}} \text{MSE}. \quad (24)$$

Since the GFT of vertex–frequency distributions has not been previously defined, firstly, we need to define the GFT of GFED. For any signal \mathbf{x} , the GFED $E_{\mathbf{x}}^a$ can be considered as a consist of N signals $E_{\mathbf{x}}^a(n, k)$, where $k = 1, 2, \dots, N$. Thus, we define the GFT of GFED as

$$\widehat{E}_{\mathbf{x}}^a = \mathbf{U}^H E_{\mathbf{x}}^a, \quad (25)$$

and its inverse as

$$E_{\mathbf{x}}^a = \mathbf{U} \widehat{E}_{\mathbf{x}}^a. \quad (26)$$

Similar to the convolution theorem in classical Fourier analysis, in GSP, we can utilize the convolution operator \star to model the filtering process. Specifically, the estimated GFED $E_{\hat{\mathbf{x}}}^a$ is obtained through the convolution of the GFED of the noisy signal \mathbf{y} and the filter \mathbf{H} in vertex-frequency domain as

$$E_{\hat{\mathbf{x}}}^a = E_{\mathbf{y}}^a \star \mathbf{H} = \mathbf{U} (\widehat{E}_{\mathbf{y}}^a \circ \widehat{\mathbf{H}}), \quad (27)$$

where \circ denotes hadamard product.

If the original signal \mathbf{x} is deterministic, \mathbf{w} is zero-mean, complex circular Gaussian noise with variance σ^2 , and \mathbf{x} and \mathbf{w} are independent, the filter transfer function matrix in the frequency-frequency domain can be derived to minimize the MSE as

$$\widehat{\mathbf{H}} = \left(\mathbb{E} \left\{ \widehat{E}_{\mathbf{y}}^a \circ \widehat{E}_{\mathbf{y}}^a \right\} \right)^{-\circ} \left(\widehat{E}_{\mathbf{x}}^a \circ \mathbb{E} \left\{ \widehat{E}_{\mathbf{y}}^a \right\} \right). \quad (28)$$

Refer to Appendix A for the detailed derivation of (28).

Thus, the optimal filter in the vertex-frequency domain can be expressed as (29).

Refer to Appendix B for the detailed derivation of (29).

By employing the optimal filter, the minimum MSE is attained in the vertex-fractional-frequency domain, resulting in optimal detection and filtering performance. The subsequent section presents experimental results that validate this optimal performance.

VII. NUMERICAL EXPERIMENTS

In this section, we conduct four numerical experiments to detect chirp signals from Examples 1–4 using the proposed graph fractional vertex-frequency energy distribution domain filtering method (GFED-F), and apply this method to several real-world datasets, thereby validating the correctness of the theory.

A. Detection of graph chirp signals

Example 3: For the signal \mathbf{x}_1 defined in Example 1, corrupted by complex circular Gaussian noise with a standard deviation of $\sigma = 0.3$, the fractional order parameter is selected as the chirp rate of \mathbf{x}_1 , with $a = 0.7$.

Example 4: For the signal \mathbf{x}_2 defined in Example 1, corrupted by complex circular Gaussian noise with a standard deviation of $\sigma = 0.3$, the fractional order parameter is selected as the chirp rate of \mathbf{x}_2 , with $a = 0.7$.

Example 5: For the signal \mathbf{x}_3 defined in Example 1, corrupted by complex circular Gaussian noise with a standard deviation of $\sigma = 0.4$, the fractional order parameter is selected as the chirp rate of \mathbf{x}_3 , with $a = 0.6$.

Example 6: For the signal \mathbf{x}_4 defined in Example 1, corrupted by complex circular Gaussian noise with a standard

$$\begin{aligned}
H(n, k) = \sum_l & \frac{\left| \widehat{E}_{\mathbf{x}}^a(l, k) \right|^2 + \sigma^2 \widehat{E}_{\mathbf{x}}^a(l, k) \sum_{i=1}^N |U_a(i, k)|^2 \overline{U(i, l)}}{\left[\left| \widehat{E}_{\mathbf{x}}^a(l, k) \right|^2 + \sigma^2 \sum_i \sum_j x(i) \overline{\widehat{x}_a(k) U_a(i, k)} |U_a(j, k)|^2 \overline{U(i, l)} U(j, l) + \sigma^2 \left| \sum_i x(i) \overline{U_a(i, k) U(i, l)} \right|^2 \right.} U(n, l) \\
& + \sigma^2 \sum_i |\widehat{x}_a(k)|^2 |U_a(i, k)|^2 |U(i, l)|^2 + \sigma^2 \sum_i \sum_j \overline{x(j) \widehat{x}_a(k)} |U_a(i, k)|^2 U_a(j, k) \overline{U(i, l)} U(j, l) \\
& \left. + \sigma^4 \left| \sum_i |U_a(i, k)|^2 U(i, l) \right|^2 + \sigma^4 \sum_i |U_a(i, k)|^2 |U(i, l)|^2 + 2\sigma^4 \sum_i |U_a(i, k)|^4 |U(i, l)|^2 \right]
\end{aligned} \tag{29}$$

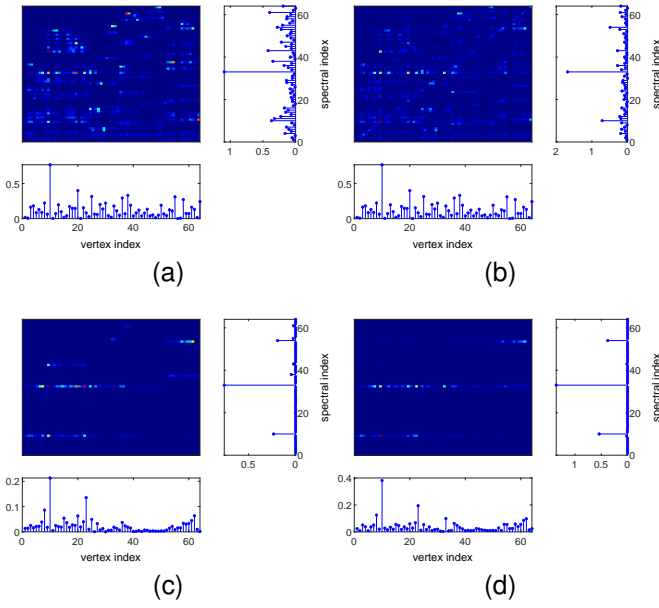


Fig. 8. Detection of graph chirp signals through filtering: Case of \mathbf{x}_1 . (a) The GED of the noisy signal. (b) The GFED ($a=0.7$) of the noisy signal. (c) The GED of the filtered signal. (d) The GFED ($a=0.7$) of the filtered signal.

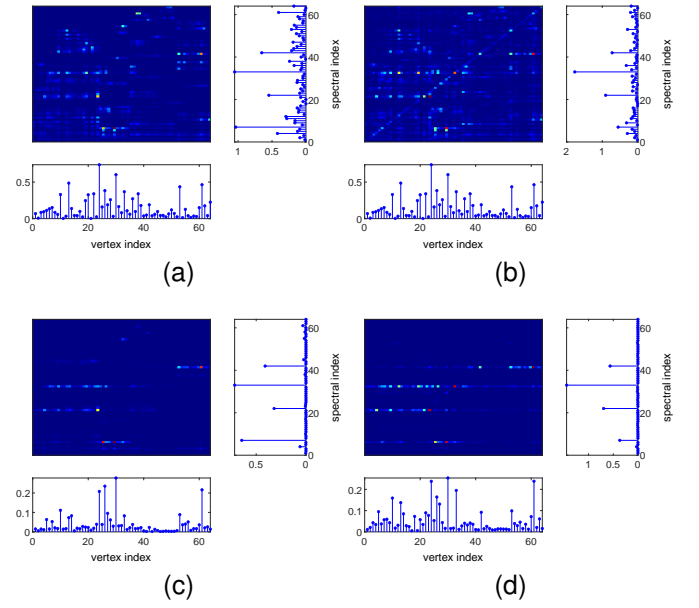


Fig. 9. Detection of graph chirp signals through filtering: Case of \mathbf{x}_2 . (a) The GED of the noisy signal. (b) The GFED ($a=0.7$) of the noisy signal. (c) The GED of the filtered signal. (d) The GFED ($a=0.7$) of the filtered signal.

deviation of $\sigma = 0.4$, the fractional order parameter is selected as the chirp rate of \mathbf{x}_4 , with $a = 0.6$.

Figs. 8–11 plot both the GEDs and GFEDs of the noisy signals in Examples 3–6, along with those of the denoised signals after filtering. As observed, the GEDs and GFEDs of the noisy signals are significantly affected by noise, making it difficult to extract meaningful signal information. However, by applying the filtering method we proposed, effective denoising can be achieved in the vertex-fractional-frequency domain, improving the detection of chirp signals. Furthermore, detection in vertex-frequency domain is less effective due to the influence of spurious frequency components, leading to analysis errors. In contrast, the vertex-fractional-frequency domain enhances signal detection performance by providing more accurate vertex and frequency information, reducing such errors and allowing for better signal representation.

B. Denoise of real-data

We also conduct experiments on five real-world datasets: sea surface temperature (SST), particulate matter 2.5 (PM-25), the thickness data on the dendritic tree, the traffic volume data for Toronto, and the Minnesota road data. The first two datasets are discussed in [42], while the latter three datasets can be accessed in [43].

For real-valued and positive signals, the vertex marginal distribution property of the GFED can be leveraged to restore the signal by performing denoising in the vertex domain. The SNR is used as the evaluation metric, calculated as $\text{SNR} = 20 \log_{10} \left(\frac{\|\mathbf{x}\|}{\|\mathbf{x} - \tilde{\mathbf{x}}\|} \right)$, where $\tilde{\mathbf{x}}$ is the filtered signal.

For the SST and PM-25 datasets, we use k -NN graph as in [42], [44] with $k = \{2, 5, 7\}$. Specifically, we use the SST data from months $T = \{50, 120, 270\}$, with zero-mean white Gaussian noise at noise levels $\sigma = \{15, 45, 60\}$. For the PM-25 data, we use data from days $T = \{50, 120, 270\}$, with zero-mean white Gaussian noise at noise levels $\sigma = \{15, 25, 35\}$. We compare the performance of the proposed

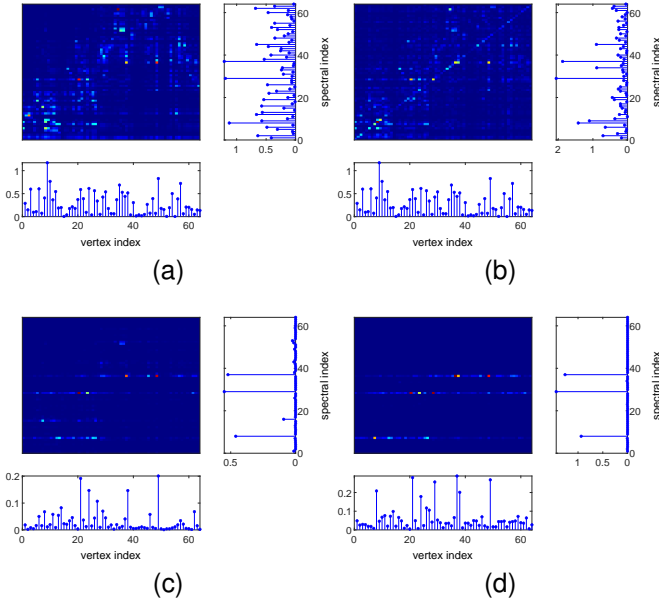


Fig. 10. Detection of graph chirp signals through filtering: Case of \mathbf{x}_3 . (a) The GED of the noisy signal. (b) The GFED ($a=0.6$) of the noisy signal. (c) The GED of the filtered signal. (d) The GFED ($a=0.6$) of the filtered signal.

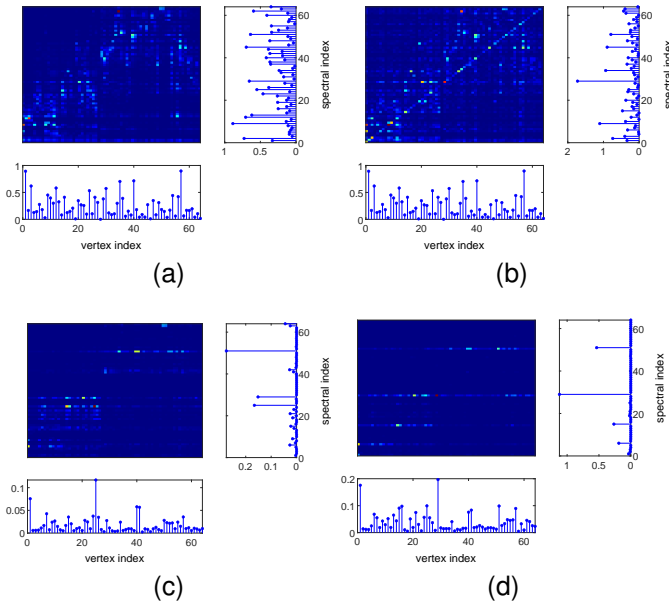


Fig. 11. Detection of graph chirp signals through filtering: Case of \mathbf{x}_4 . (a) The GED of the noisy signal. (b) The GFED ($a=0.6$) of the noisy signal. (c) The GED of the filtered signal. (d) The GFED ($a=0.6$) of the filtered signal.

GFED-F method with that of the optimal GFRT domain filtering method (OGFRFT-F) [45] at different fractional orders. Fig. 12 presents the MSE and SNR line plots of the two filtering methods under $k = 5$. As can be seen, the filtering performance of both methods changes with the fractional-order parameter a . The GFED-F generally outperforms the OGFRFT-F for most fractional-order values. In fact, for several fractional orders, GFED-F achieves better results than the optimal filtering performance of OGFRFT-F.

Additionally, Table I provides the MSE and SNR values

for both methods under the optimal parameters under $k = \{2, 5, 7\}$. In general, the GFED-F outperforms the OGFRFT-F in most scenarios. There are a few instances where OGFRFT-F shows slightly better performance. Specifically, for the SST dataset at $T = 50$ and $T = 120$ under the 7-NN graph with a noise level of $\sigma = 40$, the MSE values for GFED-F are higher than those for OGFRFT-F. Additionally, for the PM-25 dataset at $T = 50$ under 2-NN graph with a noise level of $\sigma = 15$, the MSE and SNR values for GFED-F are slightly worse than those for OGFRFT-F. In all other cases, GFED-F consistently provides better performance, highlighting its superiority over OGFRFT-F.

For the thickness data on the dendritic tree, the traffic volume data from Toronto, and the Minnesota road data, we use the same noise levels as in [46], namely 8dB, 7dB, and 5dB. Fig. 13 presents the SNR plots comparing the filtering method proposed in this paper with the GED-based Wiener filtering method (GED-WF) [46].

VIII. CONCLUSION

In this paper, we formally defined graph chirp signals, a previously undefined class of signals in GSP. We proposed the GFED to enhance the analysis of these signals, offering a more expressive representation of graph signals in the vertex-frequency domain. We explored the marginal distribution properties of GFED, further enhancing its theoretical foundation and interpretability. We also introduced the GFGD as a flexible and generalized vertex-frequency distribution, along with the reduced interference GFED, which effectively suppresses cross-terms interference and improves signal clarity. Furthermore, we proposed a graph chirp signal detection method based on GFED domain filtering and performed several experiments on graph chirp signals, demonstrating its robustness in detecting graph chirp signals under noisy conditions. Moreover, according to the marginal distribution properties of GFED, the proposed method can be applied to real-world data, showcasing its effectiveness in denoising tasks. The results confirm the effectiveness of our framework in both signal detection and noise reduction tasks, highlighting its potential for broader applications in graph signal analysis.

APPENDIX A

PROOF OF THE FILTER TRANSFER FUNCTION MATRIX (28)

Inserting (27) into (23), we can obtain

$$\begin{aligned}
 & \mathbb{E} \left\{ \|E_{\mathbf{x}}^a - E_{\mathbf{x}}^a\|_F^2 \right\} \\
 &= \mathbb{E} \left\{ \sum_n \sum_k \left| E_{\mathbf{x}}^a(n, k) - \sum_i \widehat{E}_{\mathbf{y}}^a(i, k) \widehat{H}(i, k) U(n, i) \right|^2 \right\} \\
 &= \mathbb{E} \left\{ \sum_n \sum_k |E_{\mathbf{x}}^a(n, k)|^2 \right\} \\
 &+ \mathbb{E} \left\{ \sum_n \sum_k \left| \sum_i \widehat{E}_{\mathbf{y}}^a(i, k) \widehat{H}(i, k) U(n, i) \right|^2 \right\} \\
 &- \mathbb{E} \left\{ \sum_n \sum_k \sum_i \overline{E_{\mathbf{x}}^a(n, k)} \widehat{E}_{\mathbf{y}}^a(i, k) \widehat{H}(i, k) U(n, i) \right\}
 \end{aligned}$$

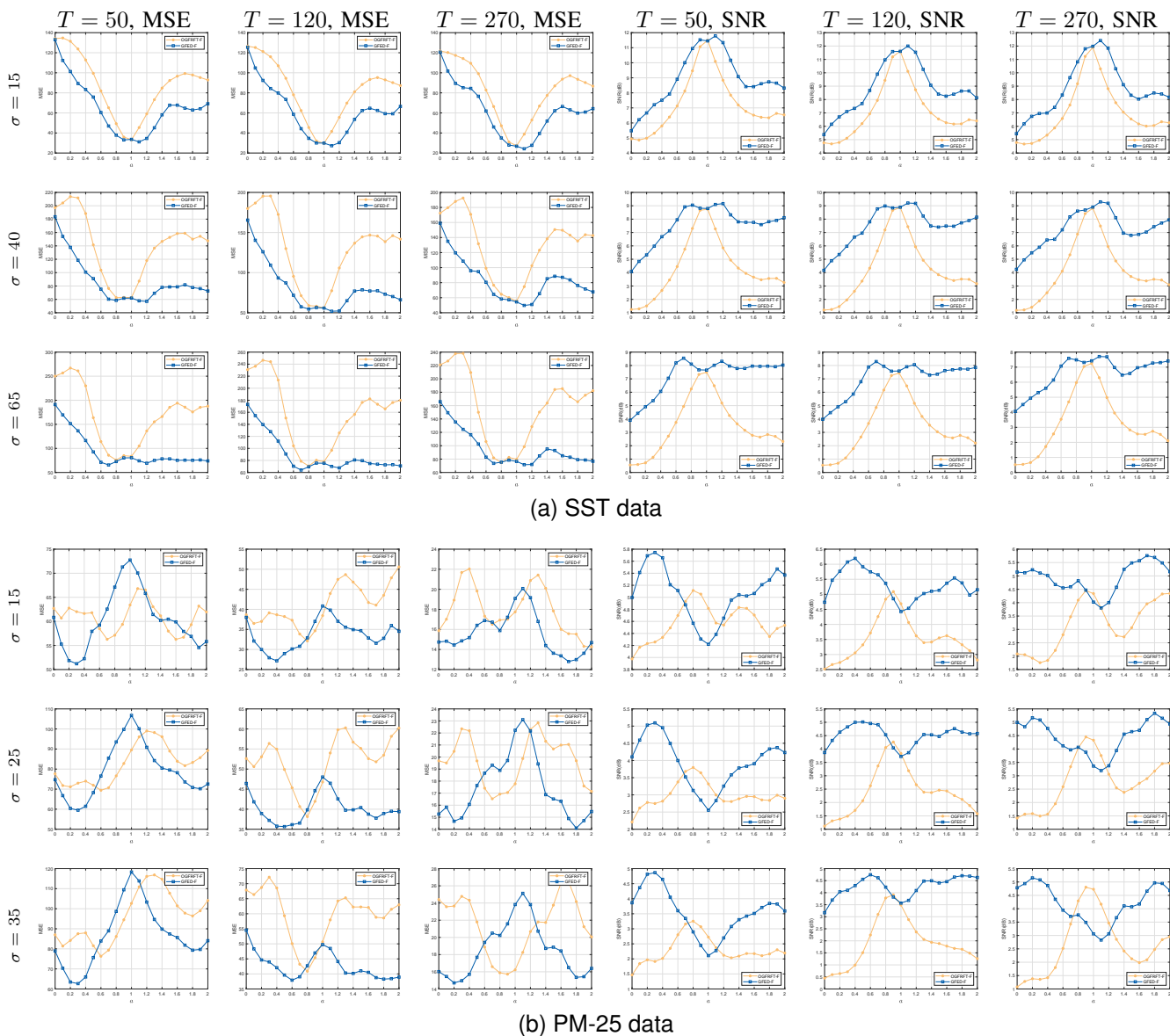


Fig. 12. Comparison of MSE and SNR line plots for OGRFT-F and GFED-F at different fractional orders using the 5-NN graph. (a) SST data with noise levels $\sigma = 15, 45, 60$. (b) PM-25 data with noise levels $\sigma = 15, 25, 35$.

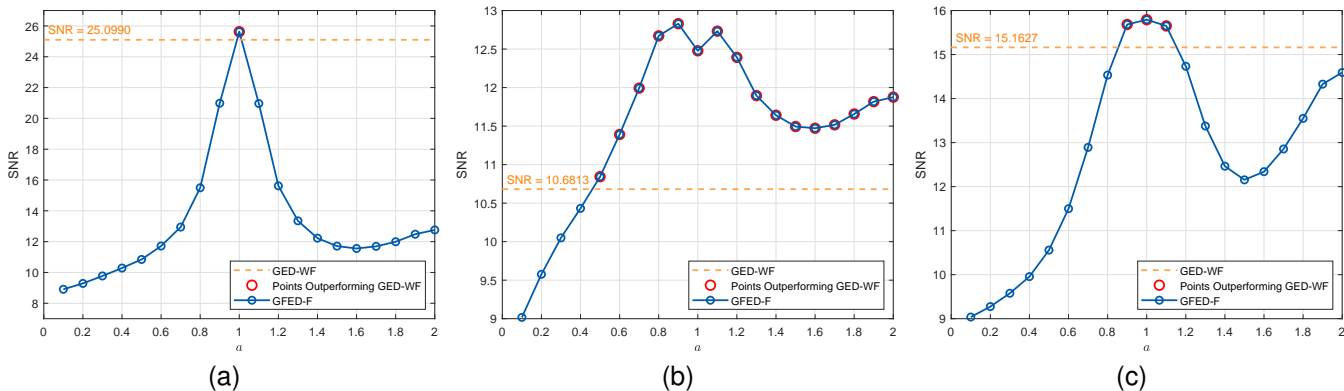


Fig. 13. Comparison of GED-WF and GFED-F. (a) Dendritic tree. (b) Toronto traffic volume. (c) Minnesota road.

TABLE I
COMPARISON OF MSE AND SNR VALUES OF SST AND PM-25 DATASETS UNDER OPTIMAL PARAMETERS OF OGRFT-F AND GFED-F.

SST	T = 50			T = 120			T = 270			
	$\sigma = 15$	$\sigma = 40$	$\sigma = 65$	$\sigma = 15$	$\sigma = 40$	$\sigma = 65$	$\sigma = 15$	$\sigma = 40$	$\sigma = 65$	
2-NN										
MSE	OGRFT-F GFED-F	49.0893 (a = 1) 45.5943 (a = 1)	165.6258 (a = 0.7) 106.9811 (a = 0.5)	178.4040 (a = 1.9) 121.7892 (a = 1.7)	49.9294 (a = 1) 46.0803 (a = 1)	160.4601 (a = 0.7) 104.1300 (a = 0.5)	170.9464 (a = 1.9) 117.0009 (a = 1.7)	51.4924 (a = 1) 49.1533 (a = 1)	166.3954 (a = 0.2) 110.5426 (a = 0.4)	178.5746 (a = 1.9) 123.8684 (a = 1.7)
SNR	OGRFT-F GFED-F	9.3684 (a = 1) 10.1287 (a = 1)	3.8365 (a = 0.7) 6.4247 (a = 0.5)	2.5915 (a = 0.6) 5.8617 (a = 1.7)	9.0481 (a = 1) 9.7233 (a = 1)	3.6820 (a = 0.7) 6.1827 (a = 0.5)	2.5120 (a = 0.6) 5.6765 (a = 1.7)	8.8801 (a = 1) 9.3421 (a = 1)	3.4858 (a = 0.7) 5.8224 (a = 0.4)	2.3535 (a = 0.6) 5.3281 (a = 1.7)
5-NN										
MSE	OGRFT-F GFED-F	33.2616 (a = 1) 31.1213 (a = 1.1)	62.6326 (a = 0.8) 56.9941 (a = 1.2)	75.8671 (a = 0.8) 65.6439 (a = 0.7)	29.7670 (a = 1) 27.2796 (a = 1.1)	56.0755 (a = 1) 51.9049 (a = 1.1)	70.7181 (a = 0.8) 64.0459 (a = 0.7)	27.2614 (a = 1) 24.2385 (a = 1.1)	55.4753 (a = 1) 49.7348 (a = 1.1)	74.6469 (a = 0.8) 71.6193 (a = 1.1)
SNR	OGRFT-F GFED-F	11.4983 (a = 1) 11.7872 (a = 1.1)	8.7418 (a = 1) 9.1595 (a = 1.2)	7.4938 (a = 1) 8.5458 (a = 0.7)	11.6211 (a = 1) 12.0000 (a = 1.1)	8.8707 (a = 1) 9.2063 (a = 1.1)	7.4377 (a = 1) 8.2935 (a = 0.7)	11.9022 (a = 1) 12.4126 (a = 1.1)	8.8167 (a = 1) 9.2911 (a = 1.1)	7.2472 (a = 1) 7.7074 (a = 1.1)
7-NN										
MSE	OGRFT-F GFED-F	28.3506 (a = 1) 28.0820 (a = 0.9)	48.5869 (a = 0.8) 52.1758 (a = 0.7)	55.8849 (a = 0.8) 52.1758 (a = 0.7)	25.8131 (a = 1) 25.3465 (a = 0.9)	45.7667 (a = 0.8) 48.8752 (a = 0.8)	53.2457 (a = 0.8) 48.8752 (a = 0.7)	23.4273 (a = 1) 22.6316 (a = 1.1)	49.7531 (a = 0.8) 49.1505 (a = 0.8)	58.1912 (a = 0.8) 55.5626 (a = 0.8)
SNR	OGRFT-F GFED-F	12.1921 (a = 1) 12.2335 (a = 0.9)	9.0967 (a = 0.9) 9.5201 (a = 0.8)	7.9153 (a = 0.9) 9.5431 (a = 0.7)	12.2400 (a = 1) 12.3192 (a = 0.9)	9.2752 (a = 0.9) 9.6220 (a = 0.8)	7.8787 (a = 0.9) 9.4675 (a = 0.7)	12.5604 (a = 1) 12.7105 (a = 1.1)	9.1663 (a = 0.9) 9.3424 (a = 0.8)	7.5997 (a = 0.9) 8.8099 (a = 0.7)
PM-25	T = 50			T = 120			T = 270			
	$\sigma = 15$	$\sigma = 25$	$\sigma = 35$	$\sigma = 15$	$\sigma = 25$	$\sigma = 35$	$\sigma = 15$	$\sigma = 25$	$\sigma = 35$	
2-NN										
MSE	OGRFT-F GFED-F	53.6247 (a = 0.1) 56.2765 (a = 0.3)	72.5014 (a = 0.1) 64.5222 (a = 0.2)	86.6515 (a = 0.1) 73.4911 (a = 0.1)	30.8939 (a = 0.3) 29.2637 (a = 0.4)	39.0386 (a = 0.4) 33.8578 (a = 0.4)	47.2836 (a = 0.5) 37.8861 (a = 0.5)	14.6532 (a = 0.9) 13.0029 (a = 0.3)	15.7741 (a = 1) 13.2016 (a = 0.2)	16.2767 (a = 1) 13.9401 (a = 0.2)
SNR	OGRFT-F GFED-F	5.4916 (a = 0.9) 5.3348 (a = 0.3)	3.7791 (a = 0.9) 4.7409 (a = 0.2)	2.7184 (a = 0.9) 4.1757 (a = 0.1)	4.1291 (a = 2) 5.8716 (a = 0.4)	2.7812 (a = 2) 5.2383 (a = 0.4)	2.2033 (a = 0.9) 4.7501 (a = 0.5)	5.0868 (a = 0.9) 5.6885 (a = 0.3)	4.3523 (a = 1) 5.6227 (a = 0.2)	4.1595 (a = 1) 5.3863 (a = 0.2)
5-NN										
MSE	OGRFT-F GFED-F	56.2678 (a = 1.6) 51.2031 (a = 0.3)	69.4473 (a = 0.6) 59.4986 (a = 0.3)	76.3163 (a = 0.6) 62.6643 (a = 0.3)	32.1141 (a = 0.8) 27.1669 (a = 0.4)	38.1410 (a = 0.8) 35.6684 (a = 0.5)	40.8834 (a = 0.8) 37.9269 (a = 0.6)	14.2646 (a = 2) 12.7965 (a = 1.7)	16.5298 (a = 0.7) 14.0974 (a = 1.8)	15.7226 (a = 0.9) 14.7062 (a = 0.2)
SNR	OGRFT-F GFED-F	5.1140 (a = 0.8) 5.7451 (a = 0.3)	3.7965 (a = 0.8) 5.0930 (a = 0.3)	3.2534 (a = 0.8) 4.8678 (a = 0.3)	5.0900 (a = 0.9) 6.1945 (a = 0.4)	4.2619 (a = 0.9) 5.0121 (a = 0.5)	3.9119 (a = 0.9) 4.7455 (a = 0.6)	4.4541 (a = 0.9) 5.7580 (a = 1.7)	4.4498 (a = 0.9) 5.3375 (a = 1.8)	5.1539 (a = 0.9) 4.8040 (a = 0.2)
7-NN										
MSE	OGRFT-F GFED-F	55.0139 (a = 1.9) 48.9340 (a = 0.3)	76.2995 (a = 0.1) 61.3034 (a = 0.3)	85.9867 (a = 0.1) 63.0833 (a = 0.3)	35.5412 (a = 0.9) 27.9296 (a = 0.5)	45.5639 (a = 1) 33.2386 (a = 0.4)	50.5346 (a = 1.1) 35.4330 (a = 1.6)	15.7331 (a = 0.1) 12.2012 (a = 0.3)	16.0110 (a = 1.3) 12.8751 (a = 0.3)	14.6749 (a = 1.2) 13.0939 (a = 0.3)
SNR	OGRFT-F GFED-F	5.3990 (a = 1.9) 5.9419 (a = 0.3)	3.2787 (a = 2) 4.9632 (a = 0.3)	2.7927 (a = 1.2) 4.8389 (a = 0.3)	5.0276 (a = 0.9) 6.0743 (a = 0.5)	3.9487 (a = 1) 5.3185 (a = 0.4)	3.4990 (a = 1.1) 5.0406 (a = 1.6)	4.1618 (a = 1.3) 5.9649 (a = 0.3)	4.3174 (a = 1.2) 5.7314 (a = 0.3)	4.8639 (a = 1.2) 5.6582 (a = 0.3)

$$- \mathbb{E} \left\{ \sum_n \sum_k \sum_i E_x^a(n, k) \overline{\widehat{E}_y^a(i, k)} \widehat{H}(i, k) \overline{U(n, i)} \right\}. \quad (30)$$

Taking the derivative of the above equation with respect to the real and imaginary parts of $H(m, l)$, we obtain

$$\begin{aligned} & \mathbb{E} \left\{ \sum_i \widehat{E}_y^a(i, l) \overline{\widehat{E}_y^a(i, l)} \widehat{H}(i, l) U(m, i) \right\} \\ &= \mathbb{E} \left\{ \sum_i \widehat{E}_x^a(i, l) \overline{\widehat{E}_y^a(i, l)} U(m, i) \right\}, \end{aligned} \quad (31)$$

which can be written as the matrix form as

$$\mathbf{U} \left(\mathbb{E} \left\{ \widehat{E}_y^a \circ \overline{\widehat{E}_y^a} \right\} \circ \widehat{\mathbf{H}} \right) = \mathbf{U} \left(\widehat{E}_x^a \circ \mathbb{E} \left\{ \widehat{E}_y^a \right\}^* \right), \quad (32)$$

and therefore, we arrive the required result (28).

APPENDIX B PROOF OF THE OPTIMAL FILTER (29)

It is obvious that

$$\mathbb{E} \{ E_y^a(n, k) \} = E_x^a(n, k) + \sigma^2 |U_a(n, k)|^2. \quad (33)$$

Thus, we have

$$\begin{aligned} \mathbb{E} \left\{ \widehat{E}_y^a(l, k) \right\} &= \mathbb{E} \left\{ \sum_{i=1}^N E_y^a(i, k) \overline{U(i, l)} \right\} \\ &= \widehat{E}_x^a(l, k) + \sigma^2 \sum_i |U_a(i, k)|^2 \overline{U(i, l)}. \end{aligned} \quad (34)$$

And $\mathbb{E} \left\{ \left| \widehat{E}_y^a(l, k) \right|^2 \right\}$ can be simplified as

$$\begin{aligned} & \mathbb{E} \left\{ \left| \widehat{E}_y^a(l, k) \right|^2 \right\} \\ &= \sum_i \sum_j \mathbb{E} \left\{ E_y^a(i, k) \overline{E_y^a(j, k)} \right\} \overline{U(i, l)} U(j, l). \end{aligned} \quad (35)$$

According to the property of zero-mean, complex circular Gaussian noise, we can obtain

$$\begin{aligned} & \mathbb{E} \left\{ E_y^a(i, k) \overline{E_y^a(j, k)} \right\} \\ &= E_x^a(i, k) \overline{E_x^a(j, k)} + \sigma^2 x(i) \overline{x_a(k)} \overline{U_a(i, k)} |U_a(j, k)|^2 \\ & \quad + \sigma^2 x(i) \overline{x(j)} \overline{U_a(i, k)} U_a(j, k) \\ & \quad + \sigma^2 |\widehat{x}_a(k)|^2 \overline{U_a(i, k)} U_a(j, k) \delta(i - j) \\ & \quad + \sigma^2 \overline{x(j)} \widehat{x}_a(k) |U_a(i, k)|^2 U_a(j, k) \\ & \quad + \sum_p \sum_q \mathbb{E} \left\{ w(i) \overline{w(j)} \overline{w(p)} w(q) \right\} \overline{U_a(i, k)} U_a(j, k) \\ & \quad \times U_a(p, k) \overline{U_a(q, k)}. \end{aligned} \quad (36)$$

Since $\mathbb{E}\{|w(p)|^2 w^*(i) w(j)\} = 0$ for $i \neq j$, $\mathbb{E}\{|w(p)|^2 w^*(i) w(j)\} = \mathbb{E}\{|w(p)|^2\} \mathbb{E}\{|w(i)|^2\} = \sigma^4$ for $i = j$, $\mathbb{E}\{|w(n)|^4\} = \mathbb{E}\left\{ [w_R^2(n) + w_I^2(n)]^2 \right\} = 2\sigma^4$, we have

$$\begin{aligned} & \mathbb{E} \left\{ \left| \widehat{E}_y^a(l, k) \right|^2 \right\} \\ &= \left| \widehat{E}_x^a(l, k) \right|^2 \\ & \quad + \sigma^2 \sum_i \sum_j x(i) \overline{x_a(k)} \overline{U_a(i, k)} |U_a(j, k)|^2 \overline{U(i, l)} U(j, l) \end{aligned}$$

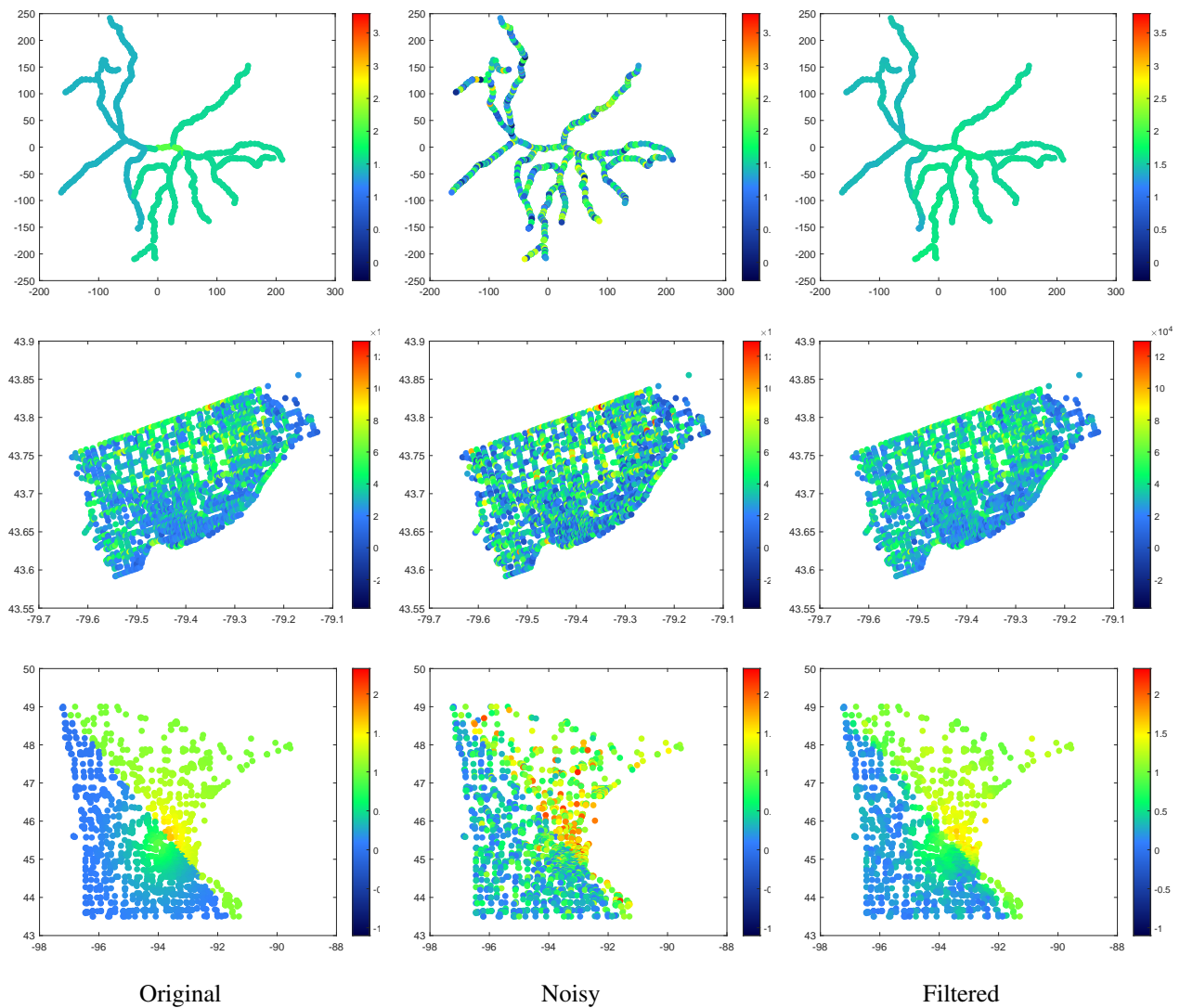


Fig. 14. The original, noisy and filtered graphs of three datasets under optimal parameters: the thickness data on the dendritic tree (top row), the traffic volume data for Toronto (middle row), and the Minnesota road data (bottom row).

$$\begin{aligned}
& + \sigma^2 \left| \sum_i x(i) \overline{U_a(i, k)} \overline{U(i, l)} \right|^2 \\
& + \sigma^2 \sum_i |\hat{x}_a(k)|^2 |U_a(i, k)|^2 |U(i, l)|^2 \\
& + \sigma^2 \sum_i \sum_j \overline{x(j)} \hat{x}_a(k) |U_a(i, k)|^2 U_a(j, k) \overline{U(i, l)} U(j, l) \\
& + \sigma^4 \left| \sum_i |U_a(i, k)|^2 U(i, l) \right|^2 \\
& + \sigma^4 \sum_i |U_a(i, k)|^2 |U(i, l)|^2 \\
& + 2\sigma^4 \sum_i |U_a(i, k)|^4 |U(i, l)|^2.
\end{aligned} \tag{37}$$

With (28), (36), and (37), we have

$$\hat{H}(l, k) = \frac{\left| \widehat{E}_x^a(l, k) \right|^2 + \sigma^2 \widehat{E}_x^a(l, k) \sum_{i=1}^N |U_a(i, k)|^2 \overline{U(i, l)}}{\mathbb{E} \left\{ \left| \widehat{E}_y^a(l, k) \right|^2 \right\}}, \tag{38}$$

where $\mathbb{E} \left\{ \left| \widehat{E}_y^a(l, k) \right|^2 \right\}$ is given by (37).

According to the inverse formula (26), we arrive the required result (29).

REFERENCES

- [1] A. Ortega, P. Frossard, J. Kovacevic, J. M. F. Moura, and P. Vandergheynst, "Graph signal processing: Overview, challenges, and applications," *Proc. IEEE*, vol. 106, no. 5, pp. 808–828, Apr. 2018.
- [2] A. Ortega, *Introduction to Graph Signal Processing*. Cambridge University Press, 2022.
- [3] G. Leus, A. G. Marques, J. M. Moura, A. Ortega, and D. I. Shuman, "Graph signal processing: History, development, impact, and outlook," *IEEE Signal Process. Mag.*, vol. 40, no. 4, pp. 49–60, Jun. 2023.

- [4] D. I. Shuman, S. K. Narang, P. Frossard, A. Ortega, and P. Vandergheynst, "The emerging field of signal processing on graphs: Extending high-dimensional data analysis to networks and other irregular domains," *IEEE Signal Process. Mag.*, vol. 30, no. 3, pp. 83–98, Apr. 2013.
- [5] A. Sandryhaila and J. M. F. Moura, "Discrete signal processing on graphs," *IEEE Trans. Signal Process.*, vol. 61, no. 7, pp. 1644–1656, Jan. 2013.
- [6] A. Sandryhaila and J. M. Moura, "Big data analysis with signal processing on graphs: Representation and processing of massive data sets with irregular structure," *IEEE Signal Process. Mag.*, vol. 31, no. 5, pp. 80–90, Aug. 2014.
- [7] L. Stankovic, D. Mandic, M. Dakovic, B. Scalzo, M. Brajovic, E. Sejdic, and A. G. Constantinides, "Vertex-frequency graph signal processing: A comprehensive review," *Digit. Signal Process.*, vol. 107, p. 102802, Dec. 2020.
- [8] L. B. Almeida, "The fractional Fourier transform and time-frequency representations," *IEEE Trans. Signal Process.*, vol. 42, no. 11, pp. 3084–3091, Aug. 1994.
- [9] H. M. Ozaktas, Z. Zalevsky, and M. A. Kutay, *The Fractional Fourier Transform With Applications in Optics and Signal Processing*. New York: Wiley, 2001.
- [10] S. Bochner and K. Chandrasekharan, *Fourier Transforms*. Princeton: Princeton University Press, 1949.
- [11] H. J. Nussbaumer and H. J. Nussbaumer, *The Fast Fourier Transform*. Berlin: Springer, 1982.
- [12] L. Stankovic and S. Stankovic, "Wigner distribution of noisy signals," *IEEE Trans. Signal Process.*, vol. 41, no. 2, pp. 956–960, Feb. 1993.
- [13] P. Djuric and S. Kay, "Parameter estimation of chirp signals," *IEEE Trans. Acoust., Speech, Signal Process.*, vol. 38, no. 12, pp. 2118–2126, Dec. 1990.
- [14] D. M. Cowell and S. Freear, "Separation of overlapping linear frequency modulated (LFM) signals using the fractional Fourier transform," *IEEE Trans. Ultrason., Ferroelect., Freq. Contr.*, vol. 57, no. 10, pp. 2324–2333, Sep. 2010.
- [15] P. R. White and J. Locke, "Performance of methods based on the fractional Fourier transform for the detection of linear frequency modulated signals," *IET Signal Process.*, vol. 6, no. 5, pp. 478–483, Jul. 2012.
- [16] A. Gavili and X. P. Zhang, "On the shift operator, graph frequency, and optimal filtering in graph signal processing," *IEEE Trans. Signal Process.*, vol. 65, no. 23, pp. 6303–6318, 2017.
- [17] Y. Q. Wang, B. Z. Li, and Q. Y. Cheng, "The fractional Fourier transform on graphs," in *Proc. Asia-Pacific Signal and Information Processing Association Annual Summit and Conference (APSIPA ASC)*, Dec. 2017, pp. 105–110.
- [18] T. Alikasifoglu, B. Kartal, and A. Koc, "Graph fractional Fourier transform: A unified theory," *IEEE Trans. Signal Process.*, vol. 72, pp. 3834–3850, Aug. 2024.
- [19] L. Stankovic, "A method for time-frequency analysis," *IEEE Trans. Signal Process.*, vol. 42, no. 1, pp. 225–229, Jan. 1994.
- [20] L. Cohen, *Time-Frequency Analysis: Theory and Applications*. Upper Saddle River, NJ, USA: Prentice Hall, 1995.
- [21] E. P. Wigner, "On the quantum correction for thermodynamic equilibrium," *Phys. Rev.*, vol. 40, no. 5, pp. 749–759, Jun. 1932.
- [22] M. Al-Sa'd, B. Boashash, and M. Gabbouj, "Design of an optimal piecewise spline Wigner-Ville distribution for TFD performance evaluation and comparison," *IEEE Trans. Signal Process.*, vol. 69, no. 6, pp. 3963–3976, Jun. 2021.
- [23] B. Boashash and P. Black, "An efficient real-time implementation of the Wigner-Ville distribution," *IEEE Trans. Acoust., Speech, Signal Process.*, vol. 35, no. 11, pp. 1611–1618, Nov. 1987.
- [24] L. Stankovic, E. Sejdic, and M. Dakovic, "Vertex-frequency energy distributions," *IEEE Signal Process. Lett.*, vol. 25, no. 3, pp. 358–362, Oct. 2018.
- [25] L. Stankovic, "The support uncertainty principle and the graph Rihaczek distribution: Revisited and improved," *IEEE Signal Process. Lett.*, vol. 27, pp. 1030–1034, Jun. 2020.
- [26] A. Rihaczek, "Signal energy distribution in time and frequency," *IEEE Trans. Inf. Theory*, vol. 14, no. 3, pp. 369–374, Jan. 1968.
- [27] L. Scharf, P. Schreier, and A. Hanssen, "The Hilbert space geometry of the Rihaczek distribution for stochastic analytic signals," *IEEE Signal Process. Lett.*, vol. 12, no. 4, pp. 297–300, Mar. 2005.
- [28] A. H. Dar, H. M. Alshambari, J. G. Dar, and S. N. Alaziz, "Novel fractional scaled Wigner distribution using fractional instantaneous autocorrelation," *Signal, Image Video Process.*, vol. 18, pp. 825–835, Apr. 2024.
- [29] M. J. Cui, Z. C. Zhang, J. Han, Y. J. Chen, and C. Z. Cao, "Convolution type of metaplectic Cohen's distribution time-frequency analysis theory, method and technology," *IEEE Trans. Inf. Theory*, pp. 1–1, Dec. 2024.
- [30] Z. C. Zhang, L. He, D. Li, Y. F. He, and W. G. Huang, "Cross metaplectic Wigner distribution: Definition, properties, relation to short-time metaplectic transform, and uncertainty principles," *IEEE Trans. Inf. Theory*, vol. 70, no. 5, pp. 3788–3822, Sep. 2024.
- [31] Z. C. Zhang, Z. C. Zhu, D. Li, and Y. F. He, "Free metaplectic Wigner distribution: Definition and Heisenberg's uncertainty principles," *IEEE Trans. Inf. Theory*, vol. 69, no. 10, pp. 6787–6810, Jun. 2023.
- [32] W. C. Zhu and Z. C. Zhang, "Instantaneous cross-correlation function- τ -Wigner distribution: Theory and application," *Signal Process.*, vol. 208, p. 108993, Jul. 2023.
- [33] P. H. Zhao and L. Xu, "Research on time domain filtering based on Choi-Williams distribution about time-phase modulation," in *Proc. 2021 7th Annual International Conference on Network and Information Systems for Computers (ICNISC)*. Guiyang, China: IEEE, Jul. 2021, pp. 708–715.
- [34] A. Rihaczek, "Signal energy distribution in time and frequency," *IEEE Trans. Inf. Theory*, vol. 14, no. 3, pp. 369–374, May 1968.
- [35] G. Quan, T. Jie, S. Huan, and W. Hong, "A novel time-frequency distribution for the short-time signal," in *Proc. 2021 4th International Conference on Information Communication and Signal Processing (ICI-CSP)*. Shanghai, China: IEEE, Sep. 2021, pp. 130–133.
- [36] Y. X. Zhao, L. E. Atlas, and R. J. Marks, "The use of cone-shaped kernels for generalized time-frequency representations of nonstationary signals," *IEEE Trans. Signal Process.*, vol. 38, no. 7, pp. 1084–1091, Jul. 1990.
- [37] X. Y. Zou, H. B. Mu, H. T. Zhang, L. Q. Qu, Y. F. He, and G. J. Zhang, "An efficient cross-terms suppression method in time-frequency domain reflectometry for cable defect localization," *IEEE Trans. Instrum. Meas.*, vol. 71, pp. 1–10, 2022.
- [38] C. S. Liang, Q. Bai, Y. Wang, Y. Gao, H. J. Zhang, and B. Q. Jin, "Spatial resolution enhancement in OFDR using Margenau Hill spectrogram," *J. Light. Technol.*, vol. 42, no. 9, pp. 3399–3408, May 2024.
- [39] J. Shi, X. J. Sha, and Q. Y. Zhang, *Fractional Order Signal Processing Theory and Methods*. Harbin: Harbin Institute of Technology Press, 2017.
- [40] R. Tao, J. M. Ma, B. Deng, and Y. Wang, *Fractional Fourier Transform and Its Applications (2nd Edition)*. Beijing: Tsinghua University Press, 2022.
- [41] L. Stankovic, E. Sejdic, and M. Dakovic, "Reduced interference vertex-frequency distributions," *IEEE Signal Process. Lett.*, vol. 25, no. 9, pp. 1393–1397, Sep. 2018.
- [42] J. Giraldo, A. Mahmood, B. Garcia-Garcia, D. Thanou, and T. Bouwmans, "Reconstruction of time-varying graph signals via Sobolev smoothness," *IEEE Trans. Signal Inf. Process. Netw.*, vol. 8, pp. 201–214, Mar. 2022.
- [43] J. Irion. [Online]. Available: https://github.com/JeffLrion/MTSG_Toolbox
- [44] T. Alikasifoglu, B. Kartal, and A. Koc, "Wiener filtering in joint time-vertex fractional Fourier domains," *IEEE Signal Process. Lett.*, vol. 31, pp. 1319–1323, May 2024.
- [45] C. Ozturk, H. M. Ozaktas, S. Gezici, and A. Koc, "Optimal fractional Fourier filtering for graph signals," *IEEE Trans. Signal Process.*, vol. 69, pp. 2902–2912, May 2021.
- [46] A. C. Yagan and M. T. Ozgen, "Spectral graph based vertex-frequency Wiener filtering for image and graph signal denoising," *IEEE Trans. Signal Inf. Process. Netw.*, vol. 6, pp. 226–240, Feb. 2020.